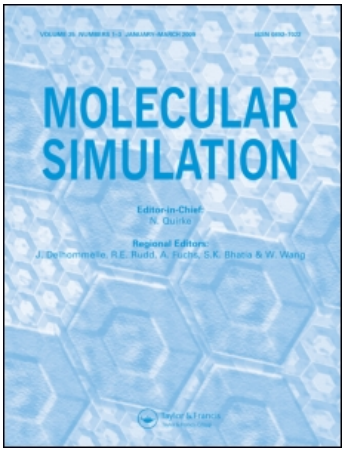

Molecular Simulation
Publication details, including instructions for authors and subscription information:
http://www.informaworld.com/smpp/title~content=t713644482

A Molecular Simulation Study of Pore Networking Effects

M. W. Maddox[a]; N. Quirke[b]; K. E. Gubbins[a]
[a] Cornell University, School of Chemical Engineering, Ithaca, New York, USA [b] Centre for Computational Chemistry Department of Chemistry, University of Wales at Bangor, Gwynedd, UK

To cite this Article Maddox, M. W. , Quirke, N. and Gubbins, K. E.(1997) 'A Molecular Simulation Study of Pore Networking Effects', Molecular Simulation, 19: 5, 267 — 283
To link to this Article: DOI: 10.1080/08927029708024157
URL: http://dx.doi.org/10.1080/08927029708024157

Molecular Simulation, 1997, Vol. 19, pp. 267–283
Reprints available directly from the publisher
Photocopying permitted by license only

A MOLECULAR SIMULATION STUDY OF PORE NETWORKING EFFECTS

M. W. MADDOX[a], N. QUIRKE[b] and K. E. GUBBINS[a]

[a]*Cornell University, School of Chemical Engineering, Olin Hall, Ithaca, New York, 14853, USA;* [b]*Centre for Computational Chemistry, Department of Chemistry, University of Wales at Bangor, Gwynedd, LL57 2UW, UK*

(Received November 1996; Accepted January 1997)

Grand canonical molecular dynamics (GCMD) simulations are used to study the adsorption and desorption of Lennard-Jones nitrogen in three slit pore junction models of microporous graphite. These networks consist of two narrow pores separated by a wider (cavity) pore. We report results for cases where the narrow pore has a width of only two or three molecular diameters. Using the GCMD technique, a novel freezing transition is observed which results in pore blocking in the narrow pores of the network, which are less than 1 nm wide. This freezing results from the adsorption energy barrier at the junction between the narrow and wider pores. This type of pore blocking could account for the apparent increase in pore volume with increasing temperature that has been experimentally observed in microporous graphite systems. For networks in which the narrower pores are somewhat larger, with a width of 1.28 nm, this pore blocking effect is much reduced, and adsorbate molecules enter and fill the central cavity. In such cases, however, desorption is incomplete, some residual adsorbate remaining in the central cavity even at the lowest pressures.

Keywords: Slit pores; pore networks; grand canonical molecular dynamics; adsorption; hysteresis

1. INTRODUCTION

Porous graphitic materials are among the most widely used and studied adsorbents available. Both the structure of these materials, and their behavior as adsorbents for a wide variety of fluids have been the subject of numerous experimental and theoretical studies. Gregg and Sing [1] have given a review of the earlier studies, including brief explanations of the observed behavior. In recent years there have been many computer simulation studies of these systems based on a simple slit pore model to

represent the porous graphite. Many of the experimentally observed properties of fluids adsorbed by porous graphite samples have been reproduced, and thus explained, by these simple adsorbent models. In reality however, a porous graphite sample is not simply an array of unconnected straight slit pores, but rather a collection of pores of different shapes and sizes, connected together to form a complex network. A straightforward elaboration of the monodisperse slit pore model involves the assumption that a porous graphitic sample consists of a distribution of unconnected straight slit pores of different sizes [2–4]. Here we present simulation results for a more complex and realistic model of a microporous graphitic sample, a slit pore junction. A simple model of a pore junction can be produced by joining together two graphitic slit pores with different pore widths. Despite the simplified nature of the model, this first step in the modeling of a graphitic pore network produces a range of novel and interesting fluid adsorption behavior associated with the junction itself.

In our preliminary work on this model [5], we used the grand canonical molecular dynamics (GCMD) technique [6,7] only for the desorption branch of the adsorption isotherm, employing regular grand canonical Monte Carlo (GCMC) methods [9] to simulate the adsorption branch. This allowed us to examine the effects of the slit pore junction geometry on desorption from a filled pore network. Here we examine three slit pore junction geometries in more detail, using GCMD to generate both the adsorption and desorption branches of the adsorption isotherm. In addition a direct comparison is made between adsorbed fluid behavior in a straight slit pore, and in the narrow pore region of the slit pore junction model. The number of GCMC steps between MD time steps is increased from 2 to 50 in order to better equilibrate regions of the network that are in contact with the bulk phase.

The use of GCMD for the adsorption branch, along with the other improvements in the model, produces different results when applied to systems similar to those studied previously. For slit pore junctions with a narrow pore region less than about 1 nm wide, a type of freezing transition occurs which is not seen in infinitely long slits of the same width. This prevents the filling of the central cavity, even after the saturated vapor pressure of the bulk fluid phase is reached. Such a transition, which occurs due to the presence of the pore junction, can provide alternative explanations for several well-known microporous behaviors. For narrow pore regions much larger than 1 nm we find that this pore blocking effect is much reduced. However, desorption is often incomplete even at very low pressures, a result of the very strong, irreversible adsorption on the walls of the cavity, and particularly in the corners where fluid-wall attraction is very

strong. These novel effects (freezing and irreversible adsorption) arise from the potential barriers at the pore junctions.

2. METHODS

Grand canonical molecular dynamics (GCMD) [6–8] is a hybrid simulation technique, incorporating aspects of grand canonical Monte Carlo (GCMC) and constant temperature molecular dynamics (MD) simulations [9]. A pure GCMC simulation uses random atom creations, deletions and displacements, whose acceptance is governed by the laws of statistical thermodynamics, to generate atomic configurations within the simulation cell. Macroscopic thermodynamic properties of the system can be calculated by averaging quantities such as the number of adsorbed atoms or the configurational energy, over several million such configurations. The creation and deletion of atoms within the system allows the number of adsorbed atoms to fluctuate, but the volume of the system, the temperature, and the chemical potential, are all fixed. The GCMC method is a natural way to simulate the adsorption of a fluid into a porous material, as the fixed parameters correspond to those of a real adsorption experiment taking place in the laboratory. Comparison between the simulation and experimental results is therefore quite straightforward. Drawbacks to the GCMC technique are that transport properties cannot be calculated, and for dense systems the creation and deletion attempts are rarely accepted, leading to poor equilibration of the system. In addition, when considering adsorption of a fluid into a porous material, GCMC creations allow atoms to adsorb into any part of the porous structure as long as the adsorption site is thermodynamically favorable, with no regard to the kinetic problem of whether the atom can circumvent physical or energetic barriers to actually get to the site.

In addition to providing transport properties, the conventional MD method generates a kinetically accurate picture of the system, with molecules being unable to move freely through physical or energetic barriers. The major problem when using such a MD simulation to model an adsorption experiment is that the number of atoms in the MD simulation cell must remain fixed. Such a closed system does not produce results that are directly comparable with experimental results (e.g. an adsorption isotherm).

The grand canonical molecular dynamics (GCMD) simulation technique takes the best aspects of both GCMC and MD, and incorporates them into a single approach. In order to do this the simulation cell must be divided into

at least two sections. In one section, regular GCMC creations and deletions are attempted, in order to fix the chemical potential and hence allow the number of adsorbed atoms in the system to fluctuate. In the case of an adsorption model, this allows the adsorbed fluid phase to equilibrate with the bulk fluid phase, as in a real experimental system. No GCMC creations or deletions are attempted throughout the rest of the simulation cell, but all the atoms in the system (including those in the GCMC section) are moved using the MD algorithm. Only the atoms in the pure MD sections of the simulation cell are included in the calculations of the thermodynamic and transport properties of the system. If such a system is correctly set up, with the GCMC section corresponding to an easily accessible region of the adsorbent, and if a large number of creations and deletions are attempted between MD timesteps, the system will remain in equilibrium with the bulk fluid phase, allowing the number of adsorbed atoms to fluctuate. Atoms in the pure MD section will provide the usual macroscopic thermodynamic quantities and a kinetically accurate picture of the adsorbed system, as well as the fluid transport properties.

The specific details of a GCMD simulation can vary, depending on the system and properties of interest. In this work we employ the constant pressure approach [6–8] to study the equilibrium adsorption of a simple fluid into a model porous adsorbent approximating a carbon slit pore with a pore junction.

The general slit pore junction geometry used in all the simulations reported here is shown in Figure 1. $L1 = 3\sigma_{ff}$ and $L2 = 7.2\sigma_{ff}$ in all cases, where σ_{ff} is the Lennard-Jones σ for fluid-fluid interactions, and each slit pore junction is defined by H/W, where H and W are pore widths defined as the distance separating the planes through the carbon atoms in the surface layer for the two opposing walls. Since we initially fix H, W is restricted to values of $H - n\Delta$, where Δ is the thickness of one graphite layer and n is an integer. Therefore a slit pore junction denoted 4/2 actually has values of $H = 4\sigma_{ff}$ and $W = 2.21\sigma_{ff}$. The GCMD code attempts to create and delete atoms only in the labeled GCMC regions. 50 attempts are made to create an atom and 50 to delete an atom in this region between each MD time step, in order to fully equilibrate the system with the bulk fluid phase. Periodic boundary conditions and the minimum image convention are employed so that the two GCMC regions are actually joined at the edge farthest from the cavity region. The rest of the simulation cell is the pure MD section, used to calculate all the results reported here. This section is further split into three parts; the cavity, pore 1 and pore 2. The cavity is the wider region of the pore junction, and the pore 1 section is the part of the narrower pore which is directly affected by the pore junction geometry at the mouth of the cavity.

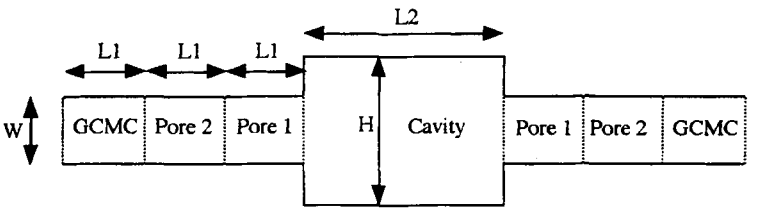

FIGURE 1 Schematic side view of the slit pore junction model, showing the sizes and positions of each region.

The pore 2 region, in contrast, is far enough from the cavity opening that a fluid atom in this region experiences essentially the same interaction with the pore wall as an atom in an infinitely long straight carbon slit pore of the same width. The fluctuation in the number of atoms in the GCMC region does not appear to adversely affect the measured properties in the pure MD region.

Three different slit pore junctions are considered here; a 4/2 junction ($H = 4\sigma_{ff}$, $W = 2.21\sigma_{ff}$), a 6/2 junction ($H = 6\sigma_{ff}$, $W = 2.42\sigma_{ff}$), and a 7/3 junction ($H = 7\sigma_{ff}$, $W = 3.42\sigma_{ff}$). In addition, the same model is used to create three straight slit pores of $H = W = 2.21\sigma_{ff}$, $H = W = 2.42\sigma_{ff}$, and $H = W = 3.42\sigma_{ff}$, for comparison with the pore 2 regions of the slit pore junction models, and for comparison with previous DFT results for Lennard-Jones (LJ) nitrogen adsorption in straight graphite slit pores. The force exerted on an adsorbed nitrogen, along with its interaction potential, is precalculated at each point in a 160 × 150 point grid for each model pore, as described previously [Maddox *et al.*, 1996]. Linear interpolation is used during the simulation to calculate the forces and potentials experienced by a nitrogen molecule at any point within the pore.

3. THE FLUID MODEL

The fluid used in our simulations is a LJ sphere with fluid-fluid parameters of σ_{ff}, = 0.375 nm and ε_{ff}/k = 95.2 K, in order to model nitrogen. The fluid-fluid interaction is cut-off at a separation of $5\sigma_{ff}$, at which distance the interaction is negligible. Nitrogen was chosen because a great number of experimental results reported in the literature use this fluid. The spherical LJ model was chosen to represent diatomic nitrogen because of the need to have an accurate equation of state [11] and saturated vapor pressure [10] for the chosen model fluid. When a bulk fluid equation of state is reported for a diatomic LJ fluid, and when this is generalized to a diatomic LJ fluid

with a quadrupole, it will be appropriate to use these more sophisticated fluid models for a study such as this.

The pore network was constructed as follows [5]. The walls consisted of an underlying smooth graphite wall, superimposed on which were atomically structured layers of graphite. In the cavity region the structureless walls were covered by just one such structured graphite layer, but in the small pore region there were two such structured layers in the case of the 4/2 network, while there were three such layers for the 6/2 and 7/3 networks. The usual parameters were used for the carbon interaction and for the layer spacing for graphite [13]. Fluid-solid interaction parameters were obtained from the Lorentz-Berthelot combining rules. The fluid-solid interaction with the underlying structureless part of the walls consisted of a 10,4,3 potential [13], and with the structured layers it was a sum of LJ potentials.

4. RESULTS

Dimensions reported here are in reduced units, denoted by an asterisk, using the LJ fluid-fluid parameters for nitrogen. Thus $H^* = H/\sigma_{ff}$, $\rho^* = \rho\sigma_{ff}^3$, $T^* = kT/\varepsilon_{ff}$ and $t^* = (m\sigma_{ff}^2/\varepsilon_{ff})^{1/2}$, where H, ρ, T, t and m are pore width, number density, temperature, time and molecular mass, respectively. The temperature was fixed at $T^* = 0.823$ ($T = 78.3$ K). Pressures are reduced with respect to the saturated vapor pressure of the same model fluid at the same temperature, P°, in a bulk system. For our studies the saturated vapor pressure of LJ nitrogen is $P^\circ = 1.47$ bar.

All simulations were performed on a Cray C90 vector processing machine at the Pittsburgh Supercomputer Center, where a typical code used 1 CPU hour to calculate the properties of an adsorption system at a single state point (fixed P, V, T), and performed at around 280 Mflops. For some state points where equilibration was particularly slow, up to 19 CPU hours were required, and for the denser systems with larger numbers of adsorbed molecules, when vector processing is at its most efficient, the peak performance reached 330 Mflops. The default timestep for the MD part of the simulation was $t^* = 0.02$, but for systems in which molecules were able to attain particularly large accelerations, t^* was reduced to 0.01, or 0.005 to prevent adsorbed molecules leaving the simulation box between timesteps. For low density systems, 500,000 MD timesteps (with 50 GCMC creation and deletion attempts between each one) were used to equilibrate the system, and another 500,000 timesteps were used to collect the averages

from which the macroscopic properties of the system were calculated. In order to optimize the usage of the available CPU time, the number of MD timesteps was reduced for higher density systems which contained more adsorbed molecules and therefore took longer to run. The minimum number of timesteps used was 100,000 for equilibration and 200,000 to collect averages. However, if the system failed to equilibrate during the initial run time, the simulation was continued until equilibration was complete. This took up to 11 million more MD timesteps (19 CPU hours) in some cases.

Adsorption isotherms were generated by performing an initial simulation using an empty slit pore junction model at a very low pressure. Once the system had equilibrated and thermodynamic properties calculated, the final configuration of adsorbed molecules was saved and then used as the initial configuration for the next simulation at a slightly higher pressure. This process was repeated until the reduced pressure was close to 1, or until no additional molecules could be adsorbed into the pore. The final configuration at the highest pressure was then used as the initial configuration for a simulation at a slightly lower pressure. This process was again repeated as the pressure was incrementally lowered, in order to investigate the desorption branch of the isotherm. This systematic approach was employed for the adsorption and desorption of LJ nitrogen at $T^* = 0.823$ in straight slit pores with reduced pore widths of 2.21, 2.43, 3.00, and 3.43, and in 4/2, 6/2, and 7/3 type slit pore junctions. Figure 2 shows the adsorption isotherms for the straight slit pores, and Figures 3–5 show those for the slit pore junctions. In addition, Figures 6–8 show a comparison of the adsorption branch for nitrogen in the 2.21, 2.43, and 3.43 straight slit pores, with the adsorption branch for nitrogen in the pore 2 region of the 4/2, 6/2, and 7/3 slit pore junctions, whose pore width is the same as those of the straight slit pores.

Initially, the GCMD method was tested against previous results [2] for LJ nitrogen adsorption in straight slit pores, calculated using density functional theory (DFT) with Steele's 10-4-3 potential [13]. The isotherms shown in Figure 2 compared very well with the DFT results at low and medium pressures, varying only slightly at the highest pressures where geometrical packing effects, which can be seen in atomistic simulations, but are harder to observe in theoretical approaches such as DFT, are probably responsible for the slight deviations.

Having verified the method and the model, we calculated the adsorption and desorption isotherms for the 4/2, 6/2 and 7/3 networks. In the 4/2 and 6/2 models, with narrow pore regions of $W^* = 2.21$ and $W^* = 2.43$ respectively, nitrogen was initially adsorbed into the narrow pore 1 and

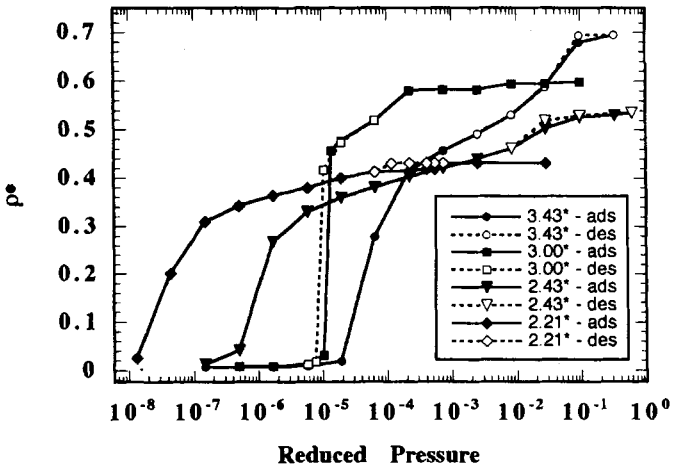

FIGURE 2 Adsorption and desorption isotherms from GCMD simulations of LJ nitrogen in straight slit pores at $T^* = 0.823$. Results for pores with reduced widths of 2.21, 2.43, 3.00, and 3.43 are shown.

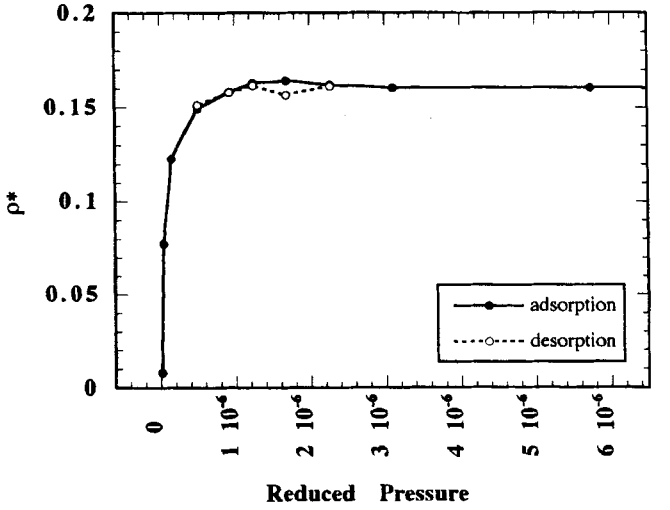

FIGURE 3 Adsorption and desorption isotherms from GCMD simulations of LJ nitrogen in a 4/2 slit pore junction at $T^* = 0.823$.

pore 2 regions, but was unable to get over the energetic barrier at the mouth of the cavity. As the pressure was increased, the pore 1 and pore 2 regions filled up whilst the cavity remained empty. A freezing transition was then observed in the adsorbed nitrogen in the narrow pore region at a reduced

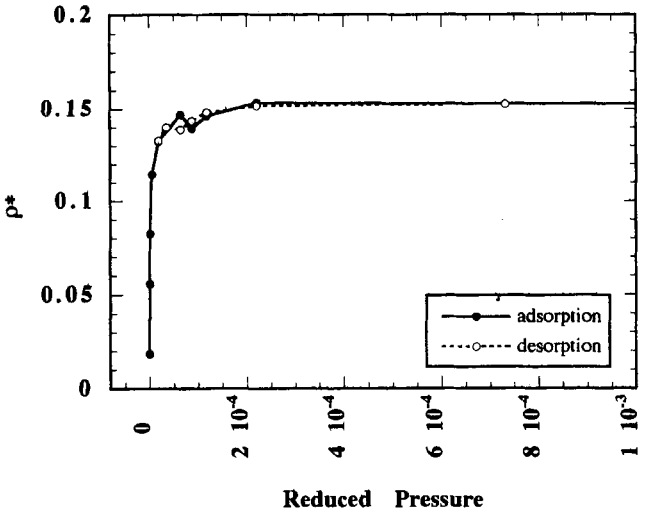

FIGURE 4 Adsorption and desorption isotherms from GCMD simulations of LJ nitrogen in a 6/2 slit pore junction at $T^* = 0.823$.

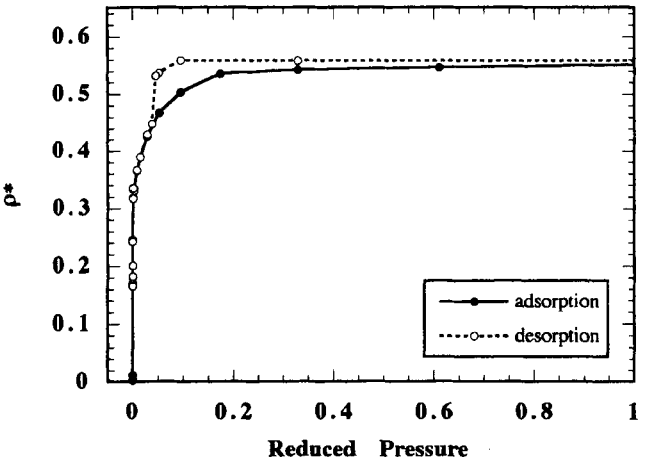

FIGURE 5a Adsorption and desorption isotherms from GCMD simulations of LJ nitrogen in a 7/3 slit pore junction at $T^* = 0.823$. Reduced pressure plotted on a linear scale.

pressure of around 2×10^{-6} for the 4/2 system and at 1×10^{-4} for the 6/2 system. No more nitrogen could be adsorbed by the slit pore junctions at higher pressures, resulting in a very low maximum adsorbed density ($\rho^* = 0.15-0.16$) due to the empty cavity region. Desorption occurred along

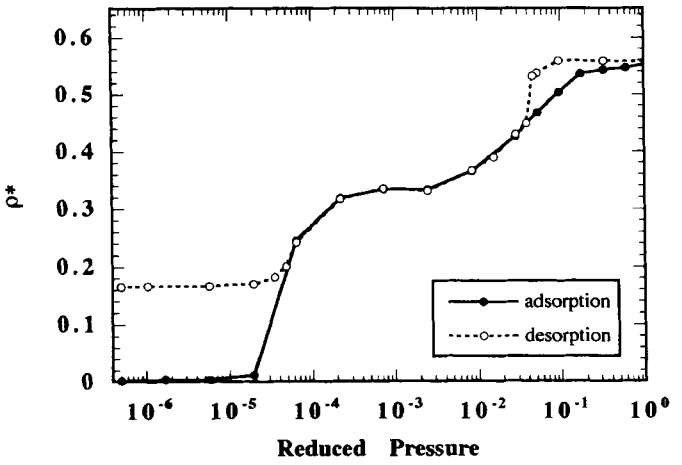

FIGURE 5b Adsorption and desorption isotherms from GCMD simulations of LJ nitrogen in a 7/3 slit pore junction at $T^* = 0.823$. Reduced pressure plotted on a log scale.

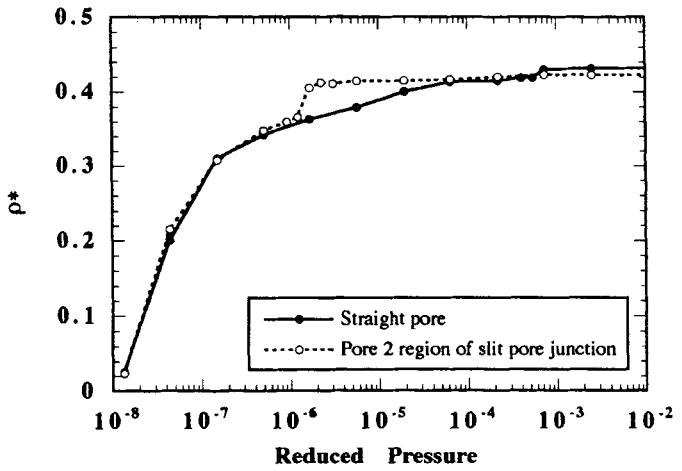

FIGURE 6 A comparison of the adsorption of LJ nitrogen in a straight pore of reduced width 2.21, and in the pore 2 region of a 4/2 slit pore junction, at $T^* = 0.823$.

almost the same path as adsorption, varying only slightly around the freezing transition. In contrast, for the 7/3 system, the energy barrier at the mouth of the cavity only prevented entry up to a reduced pressure of around 5×10^{-5}, at which point there was a slow adsorption of nitrogen molecules into the cavity, forming a rough monolayer. Adsorption then continued

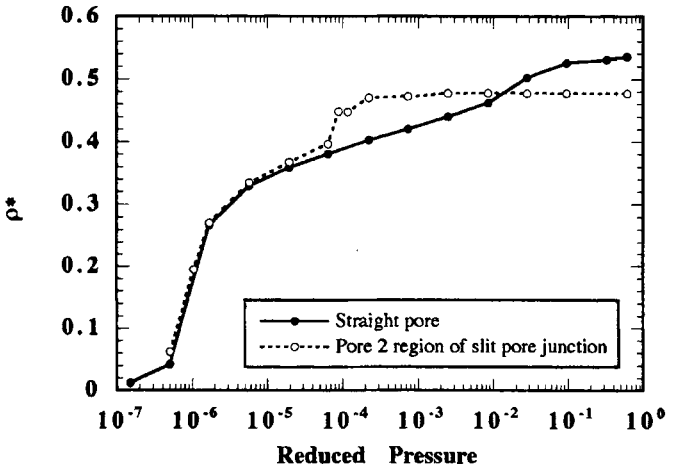

FIGURE 7 A comparison of the adsorption of LJ nitrogen in a straight pore of reduced width 2.43, and in the pore 2 region of a 6/2 slit pore junction, at $T^* = 0.823$.

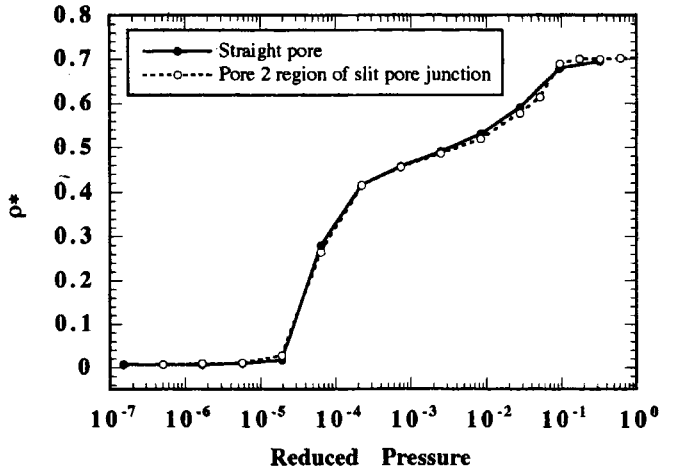

FIGURE 8 A comparison of the adsorption of LJ nitrogen in a straight pore of reduced width 3.43, and in the pore 2 region of a 7/3 slit pore junction, at $T^* = 0.823$.

throughout the system as the pressure was increased, until the cavity was almost filled at a reduced pressure of 1. The desorption branch shows a hysteresis loop at high pressure and residual adsorption at very low pressure, clearly visible in Figure 5(b). The hysteresis loop is caused by the near solid state of the nitrogen in the narrower region of the slit pore junction, through which the cavity molecules must pass in order to desorb

from the system. The residual adsorption at very low pressure is caused by the irreversible adsorption of a rough monolayer of nitrogen molecules in the cavity. Although able to surmount the energy barrier between the pore 1 region and the cavity on their way into the cavity, these molecules are unable to get over the much greater energy barrier in order to get back out of the cavity. A large increase in the temperature of the system, which provides enough thermal energy for them to get over this large energy barrier, is the only way to free these trapped molecules.

In order to examine the solidification which leads to pore blocking in the narrow region of the 4/2 and 6/2 slit pore junctions, but not in the 7/3 slit pore junction, it is useful to consider only the pore 2 region of each system. This region experiences the same interaction potential and forces due to the graphite pore as a straight slit pore of the same width. The only difference is that nitrogen molecules in this region of a slit pore junction interact with the adsorbed nitrogen molecules in other regions of the slit pore junction, which experience a different interaction with the pore wall, particularly around the opening into the cavity, and in the cavity itself. Figure 8 shows that nitrogen molecules adsorbed in the pore 2 region of the 7/3 slit pore junction behave almost identically to nitrogen molecules adsorbed in a straight slit pore of the same width ($W^* = 3.43$). In this case the solid-fluid interaction is dominant and the pore 2 region is not affected by the different behavior of nitrogen molecules in the rest of the system. Figures 6 and 7 show that at low pressure nitrogen molecules adsorbed in the pore 2 regions of the 4/2 and 6/2 slit pore junctions behave in the same way as nitrogen in a straight slit pore of the same width. The low pressure end of any isotherm is the region most affected by the details of the solid-fluid interaction, so this similarity is expected. At higher pressures, however, as the number of adsorbed molecules increases, the fluid-fluid interactions can become very important in determining the adsorption behavior of the system. In the 4/2 and 6/2 networks the density of adsorbed nitrogen in the pore 2 region abruptly increases to its capacity at a reduced pressure of around 1×10^{-6} for the 4/2 junction, and around 7×10^{-5} for the 6/2 junction; this is due to freezing of the nitrogen in the narrow pore regions. The density of adsorbed nitrogen in the straight slit, in contrast, increases smoothly all the way to its maximum value. It should be noted that the difference between the maximum adsorbed nitrogen density in the pore 2 region of the 6/2 junction and the equivalent straight slit pore is due to the way molecules in the junction are assigned to each region along a cut-off line between regions. This will only affect the reported density to any extent in very dense systems. The use of a much larger slit pore junction model, with a proportionally larger pore

2 region would yield the same maximum adsorbed density as the straight slit pore.

To investigate more closely what is happening when the adsorbed density makes this abrupt jump in the pore 2 region of the 4/2 and 6/2 slit pore junctions we considered the "cycling" of the nitrogen molecules in this region for a simulation of 200,000 MD timesteps. During a GCMD simulation, molecules are created in the GCMC region, which then diffuse throughout the system until they find their way back into a GCMC region, at which point they may be removed from the system. In a genuinely fluid system, the time taken for a molecule to make such a "cycle" is relatively short, even when the fluid is quite dense. However, as molecules become less mobile, due to solidification or entrapment within some region of the adsorbent, the time required for a cycle increases dramatically. Here we consider the fraction of adsorbed nitrogen molecules which are present in the region of interest at the beginning of a simulation run, and which remain in the pore after 200,000 MD timesteps. Comparisons of the fraction of uncycled nitrogen molecules in the pore 2 region of each slit pore junction with the fraction of uncycled nitrogen molecules in the corresponding straight slit pores are shown in Figures 9–11. Figure 11 shows that adsorbed nitrogen in the pore 2 region of the 7/3 slit pore junction behaves in essentially the same way as in the corresponding straight slit pore, remaining in a fluid state until the reduced pressure reaches about 9×10^{-2} at which point there is an abrupt change and the adsorbed nitrogen molecules are unable to diffuse into a GCMC region in order to be removed from the system. It is this solid, or very densely packed liquid nitrogen in the narrow pore region of the 7/3 slit pore junction which causes the small hysteresis loop in the isotherm at high pressure. On the adsorption branch, some molecules are still able to drop over the energy barrier into the cavity even after the "solidification" occurs in the narrow pore region, because the cavity region is still fluid and contains space to fit more nitrogen molecules. During desorption, the fluid molecules in the cavity cannot escape into the narrow pore region because this region is completely packed with molecules which are immovable until the reduced pressure "melting point" of 9×10^{-2} is reached. Therefore no molecules can desorb until the pressure falls below this value, and a hysteresis loop is the result. Since nitrogen molecules are able to surmount the energy barrier at the mouth of the cavity and almost completely populate the cavity region before the narrow pore "solidification" occurs, the overall maximum adsorbed fluid density is relatively unaffected by the narrow pore "solidification", and the only evidence of its presence is the hysteresis loop.

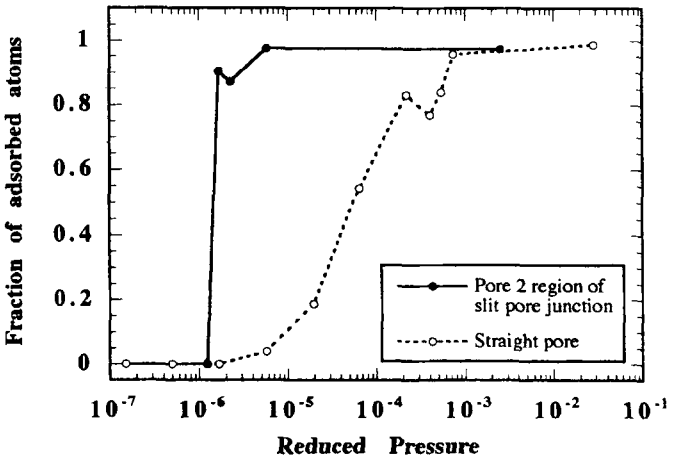

FIGURE 9 The fraction of LJ nitrogen molecules which remain in the simulation box throughout a 200,000 timestep GCMD simulation at $T^* = 0.823$. Results for a straight pore with a reduced width of 2.21 and for the pore 2 region of a 4/2 slit pore junction are shown.

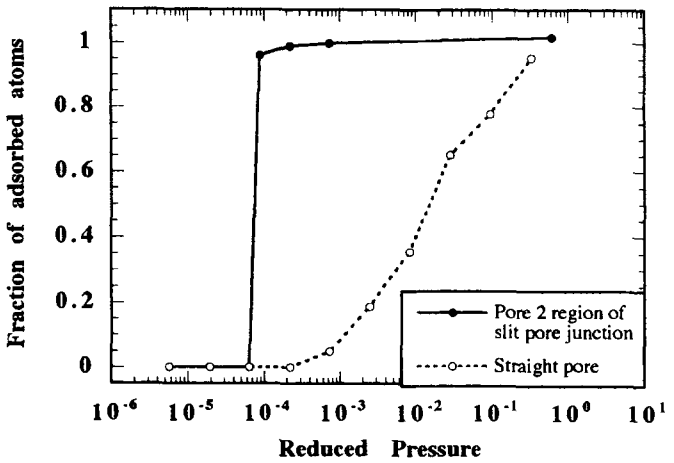

FIGURE 10 The fraction of LJ nitrogen molecules which remain in the simulation box throughout a 200,000 timestep GCMD simulation at $T^* = 0.823$. Results for a straight pore with a reduced width of 2.43 and for the pore 2 region of a 6/2 slit pore junction are shown.

The reduction of the pore width of the narrow pore region of a slit pore junction from 3.43 in the 7/3 model, to 2.43 and 2.21 in the 6/2 and 4/2 models, makes a big difference to the observed adsorbed fluid behavior. In these latter two cases, the molecules in the pore 2 region become an immobile barrier (a "solid" plug), before any molecules have entered the

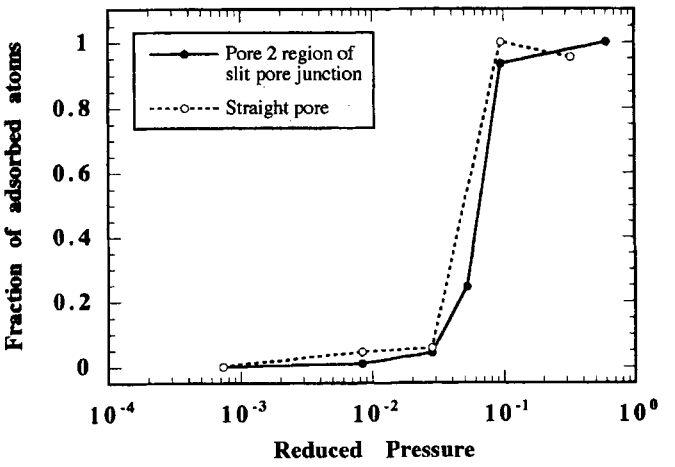

FIGURE 11 The fraction of LJ nitrogen molecules which remain in the simulation box throughout a 200,000 timestep GCMD simulation at $T^* = 0.823$. Results for a straight pore with a reduced width of 3.43 and for the pore 2 region of a 7/3 slit pore junction are shown.

cavity, and the maximum adsorbed fluid density is therefore much lower than expected. Such a measure of the adsorbed fluid density is not possible in a real system, and so an experimental study of a material containing such slit pore junctions would conclude that the porous graphite was filled with condensed fluid once the reduced pressure reached 1. This neglect of the large empty cavity would result in the assumption that the sample has a much lower capacity than in reality. Indeed, a real sample can be imagined which has large cavities connected to the bulk phase only via narrow pores which would become solid and seal off this extra internal volume before it could be filled. Estimation of the surface area and internal volume of such a sample would be very difficult, and dependent on the particular probe used, since the critical pore width, temperature and pressure at which "plugging" occurred would be sensitive to such parameters. Figures 9 and 10 show that pore filling occurs at much higher pressures in the straight slit pores than in the pore 2 region of the slit pore junction, and its onset is gradual, whereas the pore 2 regions show an abrupt change. The reason for the differences between the pore 2 region of the slit pore junctions and the corresponding straight slit pores is the presence of the energy barrier between the pore 1 region and the cavity. This energy barrier is similar to that at the open end of a straight slit pore, and it is therefore likely that a simulation of a straight slit pore with an open end would yield similar results to the pore 2 region; the usual models which utilize periodic boundary conditions are effectively

infinite in length and width, with no explicit opening to the bulk gas phase. The energy barrier at the pore junction appears to encourage the molecules behind it to pack more efficiently at a lower pressure, which not only results in the solidification of those molecules in direct contact with the energy barrier (the pore 1 region), but also any molecules in contact with those molecules (the pore 2 and GCMC regions). The ordering of the adsorbed molecules close to the energy barrier acts as a nucleus against which the rest of the adsorbed fluid can solidify at pressures far below those predicted by models without such energy barriers.

5. CONCLUSIONS

We have observed severe pore-blocking at low pressures in the narrow pores ($W^* < 2.5$) of simple slit pore junction models of porous graphite, due to the solidification of adsorbed molecules, initiated by the energy barrier at the opening to a larger cavity. Pore blocking of this type prevents the filling of any large cavities within the porous material, which are accessible only via such narrow pore networks. Since the onset of pore blocking is a function of the temperature, the unusual behavior of carbon adsorbents which appear to have an increased capacity at higher temperatures, could be explained via our model [1]. Assuming the porous network consists of many cavities of different sizes, connected to the bulk gas phase via smaller pores of different sizes, then at higher temperatures the critical pore diameter for pore blocking will be smaller, and more of the internal cavities will be accessible, thus increasing the amount of gas that can be adsorbed.

Such pore blocking behavior is not observed when the narrow pore width is increased to 3.43, because a pore of this size is able to accommodate a central layer of adsorbed molecules in addition to the monolayers at each side of the pore. This central layer adsorbs at a higher pressure than the monolayers, and does not become immobile (thus blocking the pore) until the system is close to being fully saturated.

In addition, the residual fluid in the cavity of our 7/3 slit pore junction at very low pressure indicates the irreversibility associated with the occupation of such larger cavities within the sample – another feature of the referenced example above. This residual fluid behavior, which requires a large increase in temperature to desorb the last remaining adsorbed molecules, has also been observed by Nakashima *et al.* [12].

Acknowledgements

We thank the National Science Foundation for support of this work through grants no. CTS-9508680 and INT-Supercomputer time was provided under an NSF Metacenter grant (no. MCA93S011P). Finally we thank the Pittsburgh Supercomputer Center for the use of the C90 supercomputer.

References

[1] Gregg, S. J. and Sing, K. S. W. (1982). "Adsorption, Surface Area and Porosity", 2nd ed., Academic Press, London.
[2] Lastoskie, C. M., Gubbins, K. E. and Quirke, N. (1993). "Pore size heterogeneity and the carbon slit model", *Langmuir*, **9**, 2693–2702.
[3] Lastoskie, C. M., Gubbins, K. E. and Quirke, N. (1993). "Pore size distribution analysis of microporous carbons", *J. Phys. Chem.*, **97**, 4786–4796.
[4] Lastoskie, C. M., Gubbins, K. E. and Quirke, N. (1994). Characterization of Porous Solids III, ed. by Rouquerol, J., Rodriguez-Reinoso, F., Sing, K. S. W. and Unger, K. K. Elsevier, Amsterdam, 51–60.
[5] Maddox, M. W., Lastoskie, C. M., Quirke, N. and Gubbins, K. E. (1996). Fundamentals of Adsorption, ed. by LeVan, M. D. Kluwer Academic Publishers, Boston, 571–578.
[6] Cielinski, M. M. (1985). *M. S. Thesis.*, Univ. of Maine, Orono, ME; Cielinski, M. M. and Quirke, N. (1985) unpublished.
[7] Cracknell, R. F., Nicholson, D. and Quirke, N. (1995). "Direct molecular dynamic simulation of flow down a chemical potential gradient in a slit shaped micropore" *Phys. Rev. Lett.*, **74**, 2463.
[8] Quirke, N. (1996). "Some recent developments in computational chemistry", *Mol. Sim.*, **16**, 193 208.
[9] Allen, M. P. and Tildesley, D. J. (1987). "Computer Simulation of Liquids", Oxford University Press, Oxford.
[10] Lotfi, A.,Vrabec, J. and Fischer, J. (1992). *Mol. Phys.*, **76**, 1319–1333.
[11] Johnson, J. K., Zollweg, J. A. and Gubbins, K. E. (1993). *Mol. Phys.*, **78**, 591–618.
[12] Nakashima, M., Shimada, S. and Inagaki, M. (1995). *Carbon*, in press.
[13] Steele, W. A. (1974). The Interaction of Gases with Solid Surfaces, Pergamon Press, Oxford.